Wear performance of TiC/Fe cermet electrical discharge coatings

Samer J Algodi[a,d], James W Murray[a], Paul D Brown[a,c] and Adam T Clare,[a,b]*

[a]Department of Mechanical, Materials and Manufacturing Engineering; [b]Institute of Advanced Manufacturing, Faculty of Engineering; [c]Nanoscale and Microscale Research Centre, University of Nottingham, University Park, Nottingham, NG7 2RD, UK; [d] Department of Mechanical Engineering, College of Engineering, Al-Nahrain University, Baghdad, Iraq

Abstract

The tribological behaviours of TiC-based cermet coatings, prepared by electrical discharge coating (EDC) using a semi-sintered TiC tool electrode, have been investigated. The as-deposited coatings exhibited complex microstructures, comprising TiC grains within an Fe matrix, on both high speed steel (HSS) and 304 stainless steel (304-SS) substrates. The wear resistance of TiC/Fe cermet coatings, on both substrate types, increased dramatically (one and two orders of magnitude improvement in specific wear rate), compared to as-polished substrates. Further, EDC cermet coatings on HSS were typically 2-4 times more wear resistant, depending on loading, than those deposited on 304-SS, with wear performance reflecting the composite nature of the coating coupled with the mechanical properties of the substrate. Laser surface treatments used to improve surface integrity of the as-deposited coatings, through elimination of cracks and porosity characteristic of ED coating, acted to increase wear rates for all samples, with the exception of coatings on HSS under conditions of high loading. The general increase of wear rate was attributed to a significant reduction in the proportion of TiC within the ED coatings, after laser treatment, combined with an increase in grain size; whilst improvements to the wear performance of laser treated, cermet coated HSS, under high loading, was attributed to the avoidance of an abrasive wear mechanism.

Keywords: electrical discharge coating; EDC; EDM; TiC/Fe cermet; tribology; wear

1 Introduction

The electrical discharge coating (EDC) method, being an adaptation of electrical discharge machining (EDM), may be used to produce hard cermet coatings, using a sacrificial semi-sintered tool electrode [1]. The advantages of ED processing, over competing surface modification techniques, include the ability to machine material and apply a coating using the same machine tool, without need for post-processing, combined with the ability of EDM to

create complex shapes using a shaped tool electrode, with applicability to conformal surfaces. As in EDM, the EDC plasma allows very high temperatures to be generated, beyond all material melting points. Accordingly, EDC is capable of producing coatings from hard, high melting point materials, including difficult-to-process ceramics, and hence the technique has good potential for the production of hard-wearing coatings to enhance the lifetime of complex-shaped components.

Ceramic titanium carbide (TiC) is particularly suitable for a range of wear applications, due to high hardness, high wear resistance, low coefficient of friction, and good chemical and thermal stability [2, 3]. It has been established that EDC processing using a TiC tool electrode on a stainless steel substrate yields a complex graded TiC-Fe cermet coating, resulting from a series of repeated, localised spark and melt pool formations, leading to intermixing of tool electrode and substrate material [4, 5]. There have been various reports on the formation and performance of ED TiC-based cermet coatings [6-8], however the wear behaviour of such coatings is not well understood. For example, Hwang *et al.* [6] investigated coating development using a multi-layered Ti and graphite electrode, on a Ni substrate, showing that the presence of graphite enhanced TiC layer formation, with the coating exhibiting good abrasive resistance up to ~ 400˚C, but degrading under high load conditions. Xie *et al.* [7] reported on the wear behaviour of ED coatings formed from a sacrificial Ti electrode reacting with the dielectric oil, with and without the addition of graphite powder, with a reduction in both coefficient of friction and wear rate for coatings made in the presence of graphite, being attributed to an increase in the TiC formation and to the introduction of amorphous carbon into the coatings. Further, Zeng *et al.* [8] reported improved wear performance for an ED processed TiC-N coating, as compared with a TiN physical vapour deposited (PVD) coating, for applied loads exceeding 30 N.

To date, however, there have been no systematic tribological investigations of ED coatings, and the impact of ceramic additions to the wear performance of ED processed surfaces needs to be appraised and correlated with the developed coating microstructures. In particular, it is considered that the wear behaviour of ED processed coatings is likely to be affected strongly by the integrity of the surface, *i.e.* porosity, cracks and surface roughness. One suggested approach to address this issue is to laser re-melt the coating. For example, Sova *et al* [9] reported a reduction in the porosity of cold-spray stainless steel coatings, from ~8% to ~1%, using laser re-melting. Further, Afzal *et al* [10] reported the production of plasma sprayed

WC:12%Co coatings, free of gross defects after laser melting, but with variable hardness and wear resistance as a function of laser input energy.

Here, we present a systematic study of the wear behaviour of ED processed TiC/Fe cermet coatings on two different types of steel substrates, with and without post-deposition laser melting. Wear performance for two loading conditions is investigated, correlated with near surface microstructure, to appraise the suitability of EDC to produce wear resistance coatings. Comparison is made with a reference ED machined surface, prepared using a conventional copper electrode.

2 Materials and methods

TiC-based cermet coatings and reference 'as-machined' surfaces were created using a die sinking EDM machine (Mitsubishi EA12V), using a TiC semi-sintered tool electrode (10×20×100 mm) and a pure Cu electrode (14x16x100 mm), respectively. Shell Paraol 250 oil was used as the dielectric fluid, and preferred processing parameters including electrode polarity, current, voltage, pulse-on/off time and total processing time were fixed, as summarised in Table 1 (as identified in [4]). 304 stainless steel (304-SS, 4 x 20 x 100 mm) and high speed steel (HSS, 10 x 10 x 100 mm) workpieces were mechanically polished, concluding with a 1 µm diamond paste, to a mirror finish and then washed with acetone and distilled water.

Table 1 EDC processing parameters

Working parameters	Current (A)	Pulse-on (µs)	Pulse-off (µs)	Voltage (V)	Tool electrode polarity	Machining time / minutes
Description	10	8	256	320	negative	~ 60

Table 2 Chemical composition of the starting 304-SS and HSS substrates

	C wt%	Si wt%	Mn wt%	Cr wt%	Mo wt%	Ni wt%	Al wt%	Co wt%	Cu wt%	V wt%	W wt%	Nb wt%	Fe wt%
HSS	0.87	0.39	0.30	4.26	4.21	0.17	0.03	0.23	0.07	2	5.35	0.06	bal.
304-SS	0.03	0.60	2.0	18.6	0.23	8.4	0.01	0.14	0.21	0.11	0.1	-	bal.

Substrate chemical compositions were analysed using spark emission spectrophotometry (Worldwide Analytical Systems AG, Foundry-Master; averaged over six different locations), the chemical composition of the substrates is summarised in Table 2. Coating microstructures were investigated using X-ray diffractometry (XRD) (Siemens D500, Cu Kα radiation (λ = 0.15406 nm); 40 kV and 25 mA; step size 0.02˚; step time 2 s) using a single crystal monochromator filter, scanning electron microscopy (SEM) Jeol 7100F (15 kV; spot size 8 and

10mm working distance); FEI XL30 (W-electron gun; 20 kV; spot size 4 and 10mm working distance); and energy dispersive X-ray spectroscopy (EDS) equipped with FEI XL30 (Oxford Instruments, INCA).

Wear tests were performed under dry sliding conditions using an in-house linear reciprocating ball-on-flat tribometer. Preliminary experimentation established suitable room temperature wear test parameters for this study of 10k and 35k cycles, at a frequency of 2 Hz, with normal applied loads of 10 N and 50 N, with constant wear track length set at 10 mm. No further surface preparation was conducted on the samples prior to wear testing. All wear tests were repeated three times, each using a new alumina (Al_2O_3) ball (9.525 mm). Surface roughness and transverse line profiles of the wear tracks were obtained using a Talysurf series CLI 1000 (Taylor Hobson) profilometer with an inductive type contact stylus (lateral resolution 0.5 µm). Five profiles were recorded for each wear trace, each separated by a distance of ~ 2 mm, before averaging. Based on the volume loss V (mm^3), the specific wear rate W (mm^3/Nm) was calculated according to Equation 1.

$$W = \frac{V}{2L\,S\,N} \qquad (1)$$

Where L (N) is the applied load, S (mm) is the stroke length, and N is the total number of reciprocations. Wear rates of the counterbodies were calculated using area measurement of optical micrographs of the associated wear patches, and volume measured using the equation for volume of a sphere.

EDC processed surfaces subjected to an additional laser surface treatment (LST), to homogenise the near surface microstructure, were also investigated, using a 2 kW Ytterbium fibre laser (IPG Laser Company; model YLR-2000; continuous-wave (CW); wavelength ~1070 nm; lens - workpiece separation 192 mm; spot size 1 mm; scan speed 1600 mm/min). Laser powers of 240 and 280 W, corresponding to fluences of 9 and 10.5 J/mm^2, respectively, were identified on the basis of preliminary experimentation to identify processing conditions suitable for material melting. LST was performed under an inert atmosphere of Ar gas. Scans were performed line by line, with track overlaps of 60%, to ensure the entirety of the processed surfaces remelted.

3 Results

3.1 Coating and machined-surface microstructures

Figures 1a-d present secondary electron (SE) micrographs of the TiC/Fe cermet coating and reference Cu EDM samples, on 304-SS and HSS substrates, respectively. The development of micro-cracks along with void formation was evident for all these processed samples. The average roughness of cermet coated 304-SS (Ra ~ 1.3 μm) was slightly higher than that of the coated HSS (Ra ~ 1.2 μm) samples. Further, EDS analyses of the cermet coated surfaces revealed Ti incorporations, *i.e.* corresponding to TiC transferred from the tool electrode, of ~ 39.4 wt% and ~ 29.3 wt% into the 304-SS and HSS, respectively. For comparison, 304-SS and HSS samples EDM processed using a conventional Cu electrode similarly exhibited distributed cracking and void formation (Figures 1b,d), with the delineation of final craters produced by the discharge process. In this case, average surface roughness values of 1.2 μm and 1.6 μm were returned for the processed 304-SS and HSS samples, respectively.

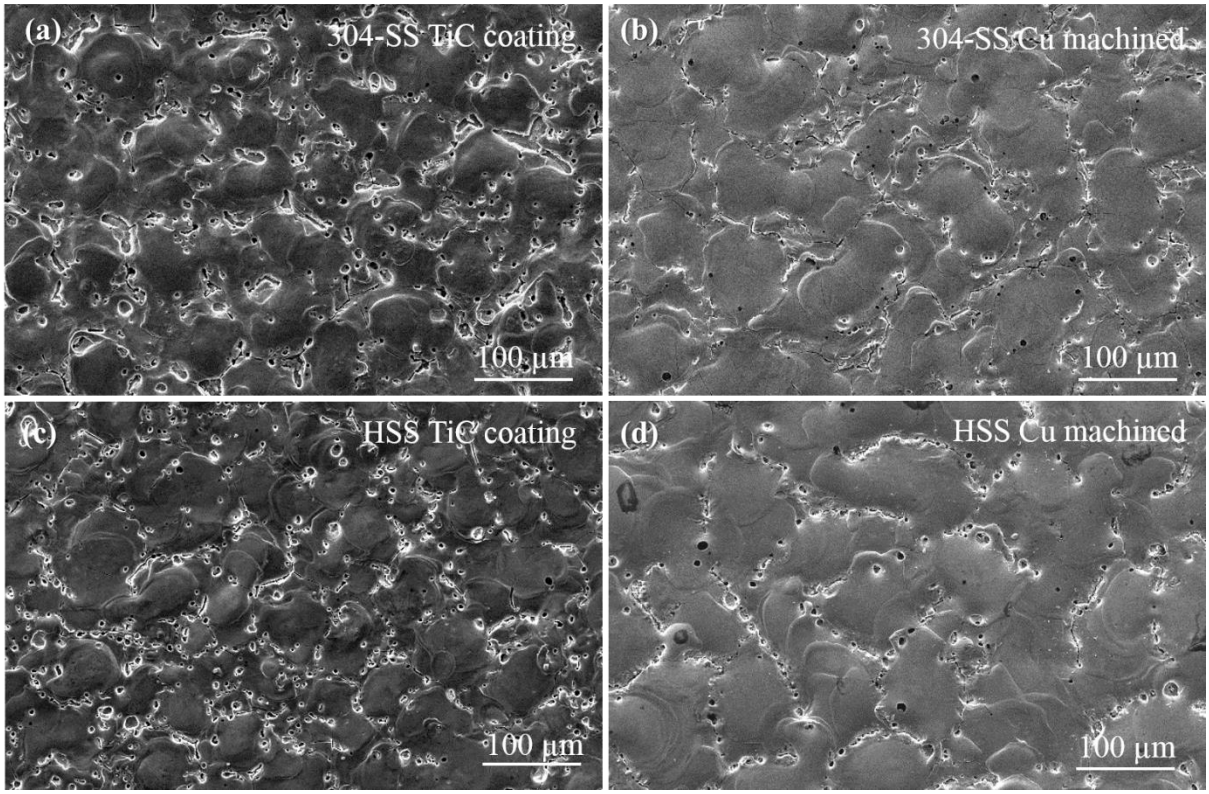

Figure 1 SE images of (a,c) ED cermet coatings; and (b,d) EDM Cu reference samples on 304-SS and HSS substrates, respectively.

Figure 2 presents backscattered electron (BSE) images of the TiC/Fe cermet ED coating on a 304-SS substrate (cf. Figure 1a), viewed in cross-section, showing the development of an irregular, banded, composite microstructure. TiC grains appear dark in BSE imaging, indicative

of the low, locally averaged, mean atomic number of TiC compared to Fe. The complicated microstructure varies as a function of depth into the coating (Figure 2b), reflecting the final cool-down sequence of the processed ED coating [11], with a mixture of equiaxed and banded columnar grains near the surface (Figure 2c) and coarse to finely graded equiaxed grains towards the coating / substrate interface (Figure 2d). The presence of ~ 21% Fe within the coating (as determined by EDS, see also Table 3) is indicative of the extent of intermixing of substrate and tool electrode material [4, 5]. The coating is also characterised by crack formations (*e.g.* Figure 2a, arrowed), and also the incorporation of some significantly larger TiC particles (*e.g.* Figure 2d, arrowed), being attributed to unmelted TiC, incorporated into the molten coating during processing.

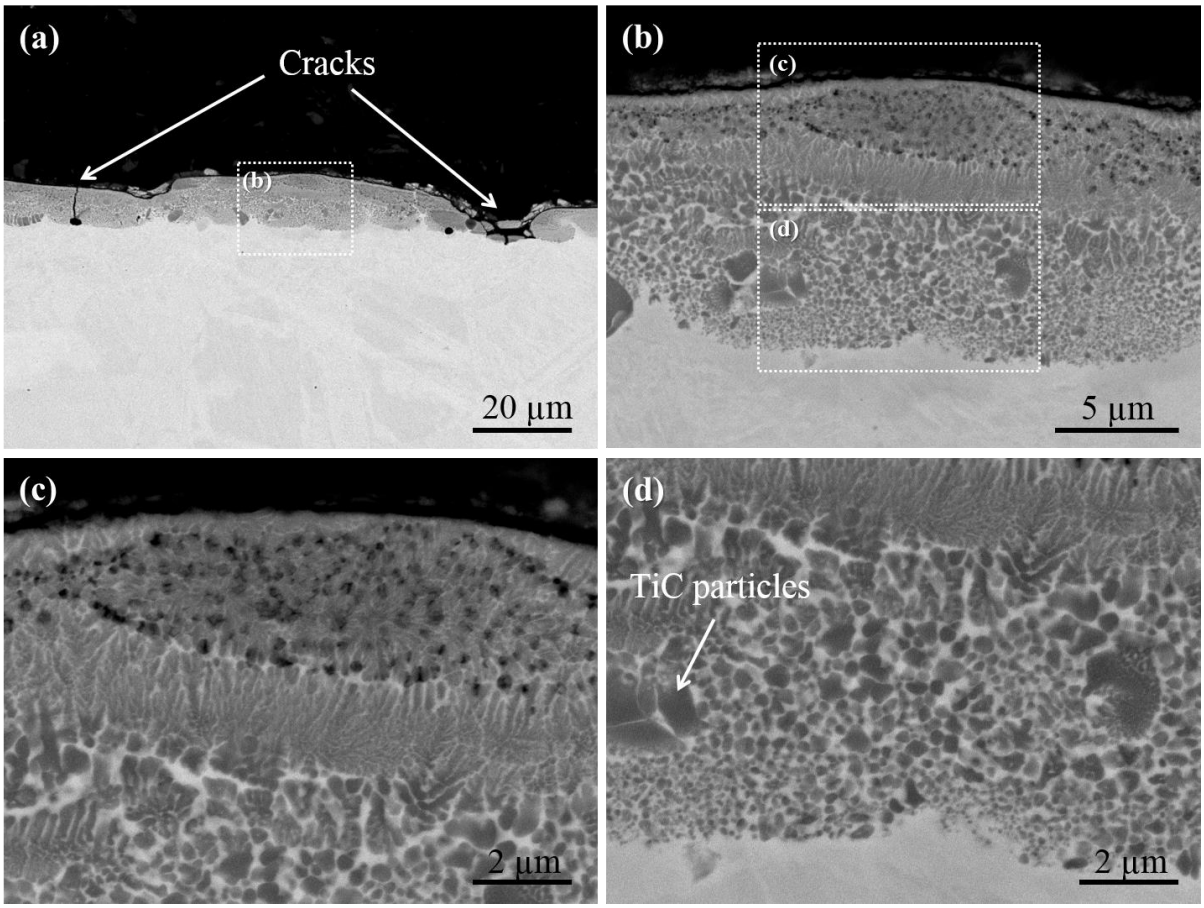

Figure 2 Cross-sectional BSE images of a TiC/Fe cermet ED coating on 304-SS (TiC deposited under conditions of 10 A current and 8 µs pulse-on time), showing the development of a banded, composite microstructure.

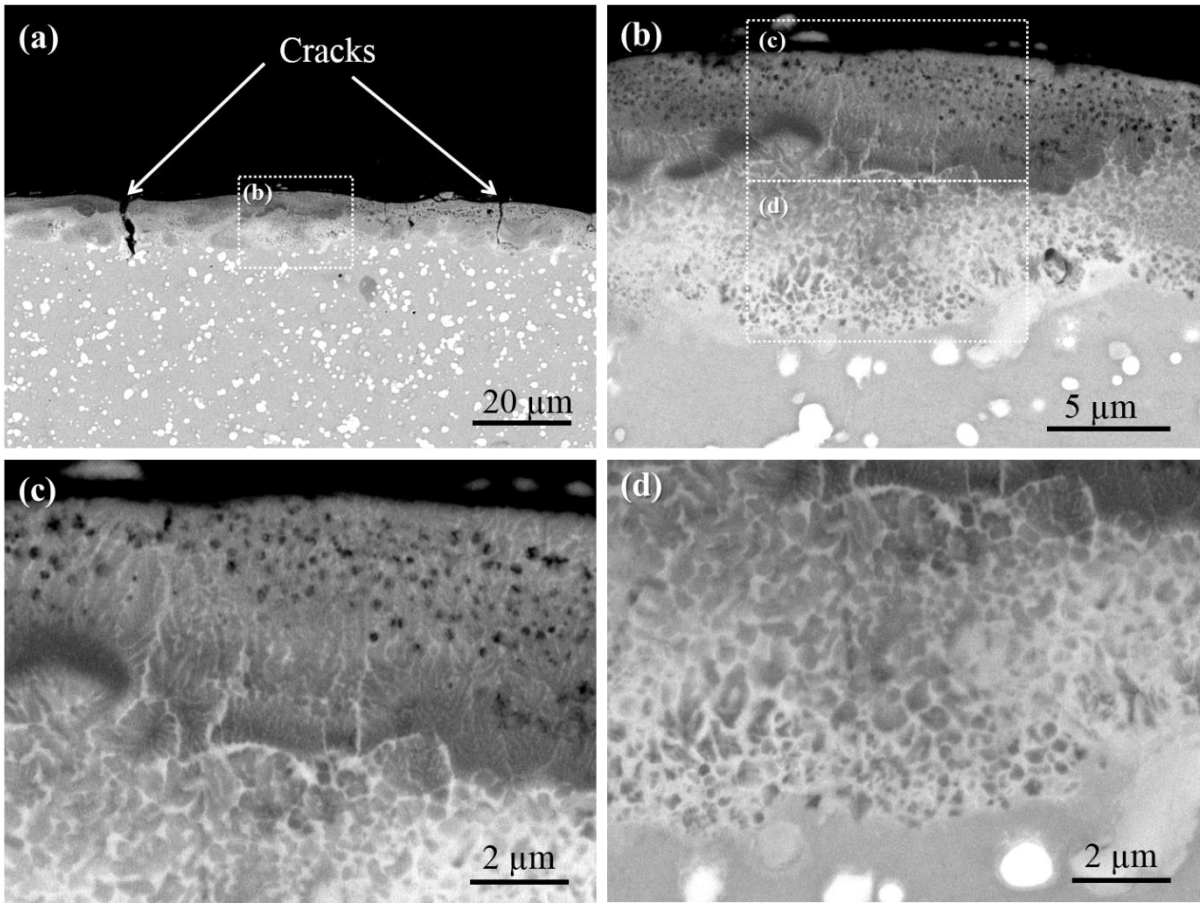

Figure 3 Cross-sectional BSE images of a TiC/Fe cermet ED coating on HSS (TiC deposited under conditions of 10 A current and 8 µs pulse-on time), showing the development of a similar, variable, composite microstructure.

Figure 3a-d presents BSE images of the TiC/Fe cermet ED coating on the HSS substrate, showing the development of a similar, irregular, composite microstructure. Again, the microstructure varies with depth into the coating (Figure 3b), with local variations of equiaxed and columnar grains reflecting the cool-down sequence of the final intermixed molten layer (Figures 3c,d), with ~ 30% Fe within the coating in this instance (Table 3). The coating was again characterised by significant crack formations (*e.g.* Figure 3a, arrowed).

Complementary XRD analyses were performed to appraise the crystal structures of the steel substrates and the ED processed samples (Figure 4). Figure 4a presents XRD patterns for the as-polished 304 stainless steel substrate, the as-deposited TiC/Fe cermet coating, and a reference machined surface. The substrate diffraction pattern revealed peaks due to the dominant austenite (γ) phase with some martensite (α'), with the latter indicative of the effects of cold working [12]. The reference surface machined using the Cu electrode again showed the dominance of cementite (Fe_3C), due to reaction between Fe from the substrate and cracked

carbon from the dielectric (hydrocarbon) oil, along with some austenite (γ) and low intensity peaks due to martensite (α′) and Cr_3C_2. The XRD pattern for the developed cermet coating exhibited six dominant peaks consistent with the presence of TiC, demonstrating conservation of TiC particles from the semi-sintered tool electrode into the workpiece surface, along with peaks due to austenite (γ), martensite (α′) and graphite.

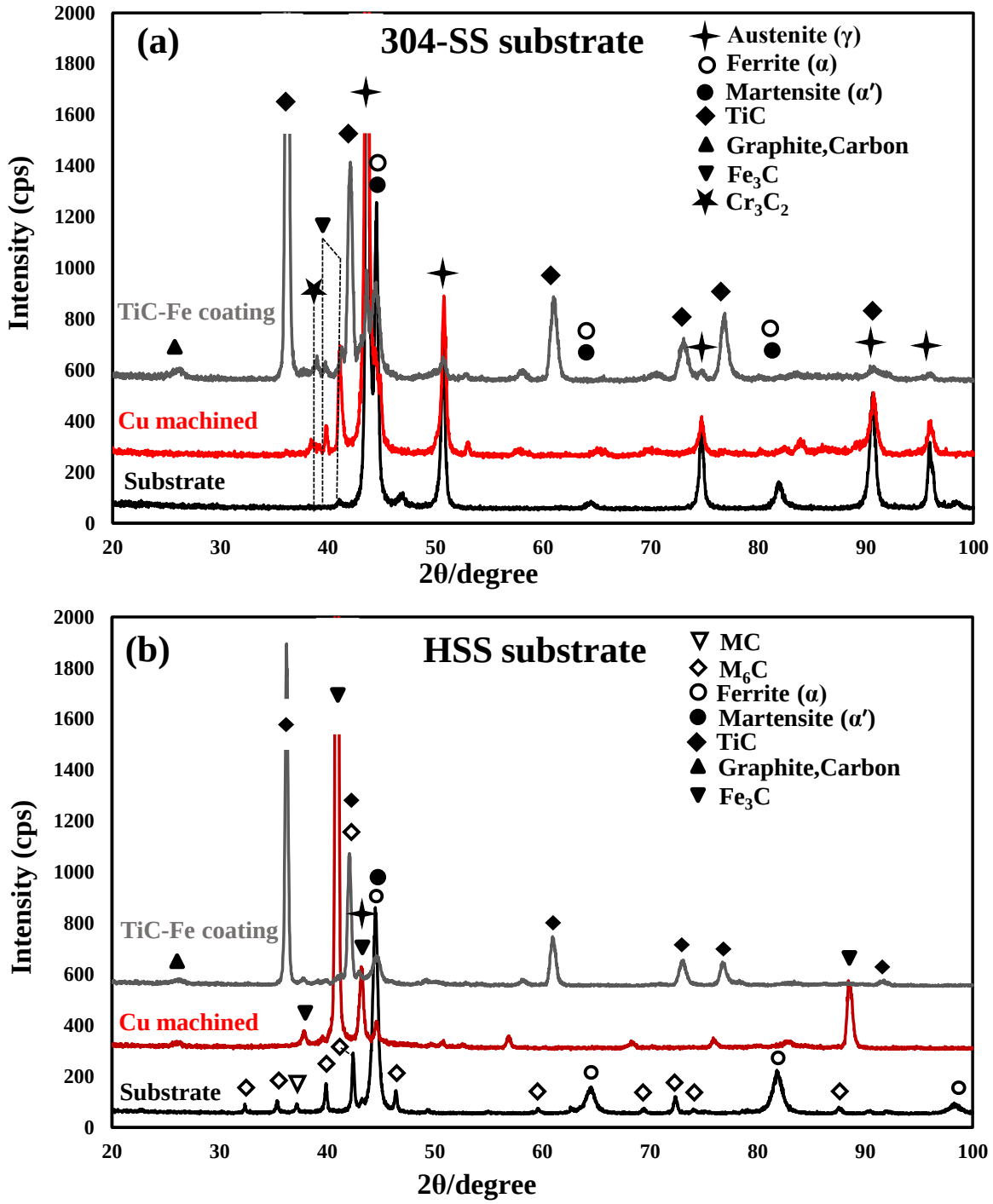

Figure 4 XRD patterns for ED processed TiC/Fe cermet coatings on (a) 304-SS and (b) HSS substrates, along with reference Cu machined surfaces.

Figure 4b similarly presents XRD patterns for the as-polished HSS substrate, the as-developed TiC/Fe cermet coating, and a reference Cu ED machined surface. In this case the HSS substrate was comprised mainly of ferrite (α) and M_6C carbide (Fe-Mo-C), with evidence of MC vanadium rich carbide (V-C) peaks. For the case of the reference surface processed using a solid Cu electrode, XRD revealed the dominance of cementite (Fe_3C). Minor peaks attributable to ferrite (α) phase or martensite (α′) were detected also, recognising the difficulty of distinguishing between these two phases possessing the same diffraction peaks [13]. No Cu-based phases were detected. EDC samples prepared using the TiC electrode exhibited dominant diffraction peaks due to the TiC phase, in addition to a smaller peak attributable to ferrite (α) or martensite (α′), along with a signature for austenite (γ).

3.2 Reciprocating wear testing

3.2.1 Specific wear rates and wear scar profiles

As-processed TiC/Fe cermet coatings, on both substrate types, were wear tested using a dry sliding reciprocating technique, under conditions of 10 N and 35,000 reciprocating cycles, and 50 N and 10,000 cycles, respectively. Specific wear rates (Figure 5) were determined from the cross-sectional profiles of the wear tracks.

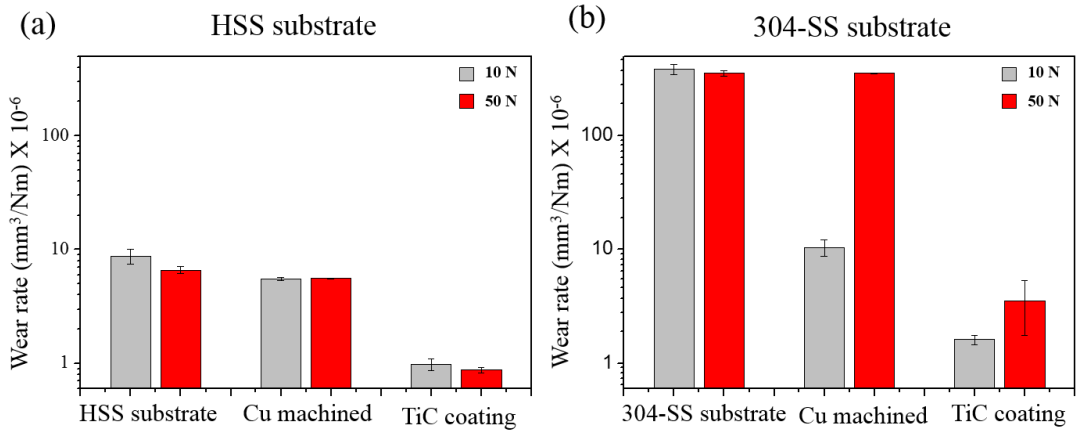

Figure 5 Specific wear rates (logarithmic scale) for samples based on: a) HSS and b) 304-SS substrates (as-polished substrate; EDM Cu reference surface; and EDC TiC/Fe cermet coating) under loads of 10 N and 50 N, respectively.

The wear rate for the TiC/Fe cermet coated HSS sample was approximately an order of magnitude lower than that of the as-polished HSS substrate, under loads of both 10 and 50 N

(Figures 5a). Further, the wear rate of the cermet coated 304-SS, outperformed the as-polished substrate by approximately two orders of magnitude (Figures 5b), again demonstrating that the EDC coating provides significant tribological benefit, under both loading conditions. Even though the 304-SS substrate benefits more than the HSS, in practical terms, from the EDC process, the absolute wear rate of the coating on 304-SS was slightly higher (~ 2-4x) than that on HSS, indicating a combined effect of coating and substrate on the wear mechanism. It is note that the reference Cu EDM machined HSS surface yielded no significant improvements in wear behaviour, compared to the as-polished substrate, for both loading conditions (Figure 5a), whilst interestingly the Cu EDM machined 304-SS sample yielded an order of magnitude improvement in specific wear rate under loading conditions of 10 N, but no improvement under conditions of 50 N (Figure 5b).

Figure 6a-d presents cross-sectional profiles of the wear tracks for the as-polished substrates, EDM Cu reference samples, and EDC TiC/Fe cermet samples, on HSS and 304-SS, under conditions of 10 and 50 N, respectively. It is interesting to note that as-polished 304-SS substrate showed very wide and deep wear tracks, which were replicated following EDM Cu processing under a 50 N load (Figure 6d), whilst the wear profiles were much shallower under a reduced load of 10 N (Figure 6c). Conversely, better wear resistance was shown by the as-polished HSS substrates, although very similar wear profiles were returned following EDM Cu processing, for both loading conditions of 10 and 50 N (Figures 6a and b). Most importantly and in all cases, however, the TiC/Fe cermet coating showed much shallower, narrow wear track profiles (Figure 6, grey lines), indicative of small amounts of material removal and vastly superior wear resistance in comparison to the as-polished substrate and Cu machined surfaces.

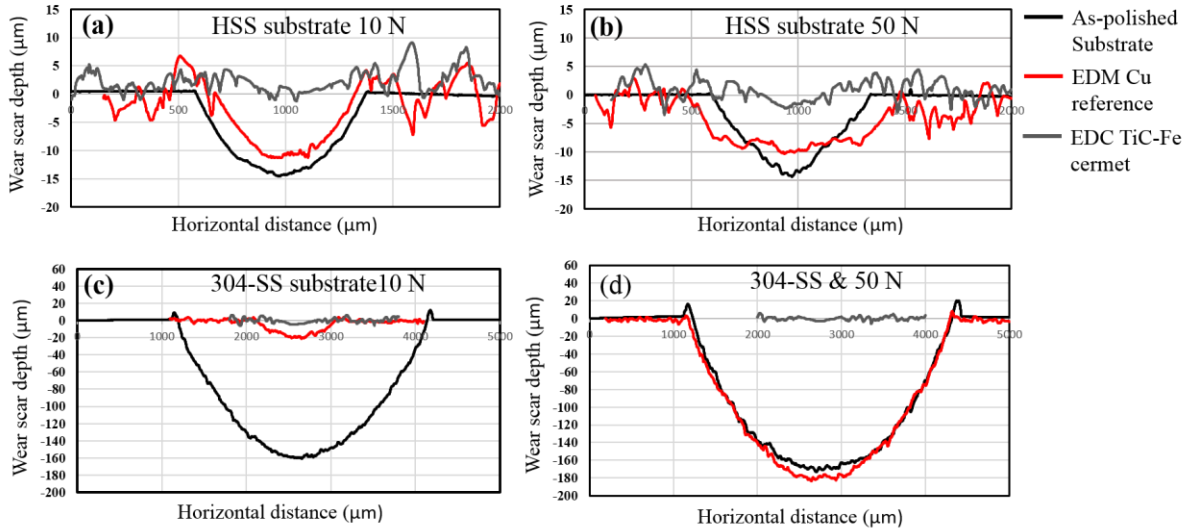

Figure 6 Cross-sectional wear scars profiles for the as-polished substrates, EDM Cu reference samples, and EDC TiC/Fe cermet samples: a,b) HSS and c,d) 304-SS, both under conditions of 10 and 50 N, respectively.

3.2.2 Wear scar characterisation

Low and representative high magnification SEM imaging of the wear scars was performed in order to gain improved understanding of the wear mechanisms of these processed samples. Figure 7 presents mixed secondary electron (SE) and backscattered electron (BSE) images of the wear track (Figure 7a) and highlighted details (Figure 7b,c) of the as-polished HSS under conditions of 10 N load. The surface shows a uniform wear track, with parallel scratches along the sliding direction (Figure 7c), combined with accumulated wear debris at the ends of the reciprocating track [14], being indicative of abrasive wear [15, 16]. Further, EDS analyses of the wear debris indicated enhanced levels of oxidation (O ~ 16.4 wt% and 30.0 wt%; Figure 7b, regions II and III, respectively), as compared to the as-polished substrate (O ~ 1.43 wt%; (Figure 7b region I)).

The development of a cermet coating leads to an increase in the hardness of the near surface modified layer [4], resulting in enhanced wear resistance of the substrate. For example, Figure 8 illustrates a wear track (Figure 8a) and associated details (Figure 8b and c) of the cermet coating on HSS under 10 N loading. In this case, the wear track shows a uniform, smooth surface, along with some cracks and voids associated with the initial as-developed EDC coating (Figures 8b,c).

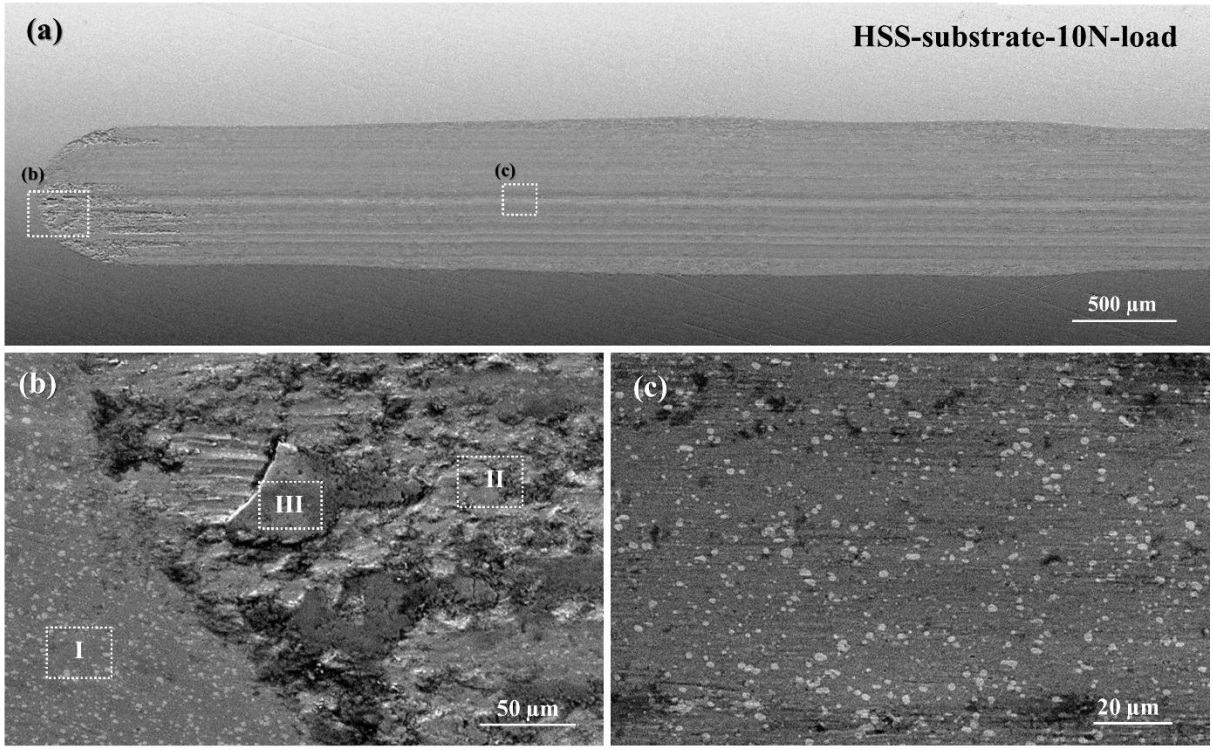

Figure 7 Low magnification SEM images showing (a) the extent (mixed SE & BSE image) and (b,c) representative details of a wear scar on an as-polished HSS substrate under loading conditions of 10 N, indicative of abrasive wear (SE image).

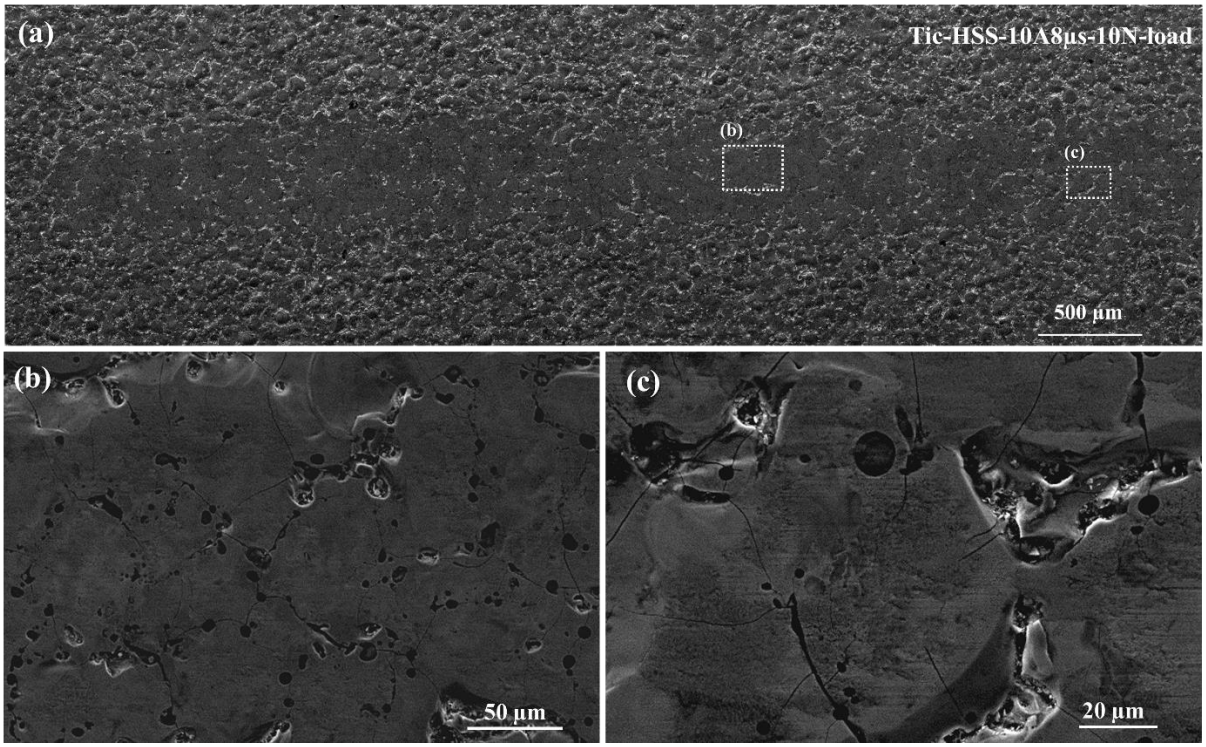

Figure 8 Low magnification SE images showing (a) the extent and (b,c) two representative details of a wear scar on a cermet coated HSS sample, under loading conditions of 10 N, indicative a greatly improved wear performance.

For completeness, Figures 9 and 10 presents high magnification SE images of wear track details on the HSS and 304-SS substrates, under conditions of 10 N and 50 N loading, respectively, for comparison of the as-polished substrates, the EDM Cu reference samples, and the ED processed TiC/Fe cermet coatings.

The as-polished 304-SS (Figure 9b) under 10 N loading shows evidence of a more severe wear regime, compared to HSS (Figure 9a), with regions of embedded wear particles, indicative of adhesive wear [17, 18]. However, the wear tracks on both cermet coated HSS and 304-SS substrates under low loading conditions showed very similar, improved wear morphologies (Figures 9e and 9f, respectively), with the development of more uniform, smooth wear surfaces, again with cracking and voids from the initial EDC coating. Intriguingly, the HSS reference sample, EDM processed with a Cu electrode, under 10 N loading, generally shows a smooth surface, along with some localised regions of high oxygen level indicative of an oxidation mechanism (Figure 9c). Conversely, the 304-SS sample EDM processed reveals a different wear mechanism including abrasive grooves as well as delamination (Figure 9d), again suggesting an adhesive mode of wear. Further, some cracks and voids associated with the initial EDM process were evident for both substrates (Figures 9c,d), along with debris deposited near the wear track ends.

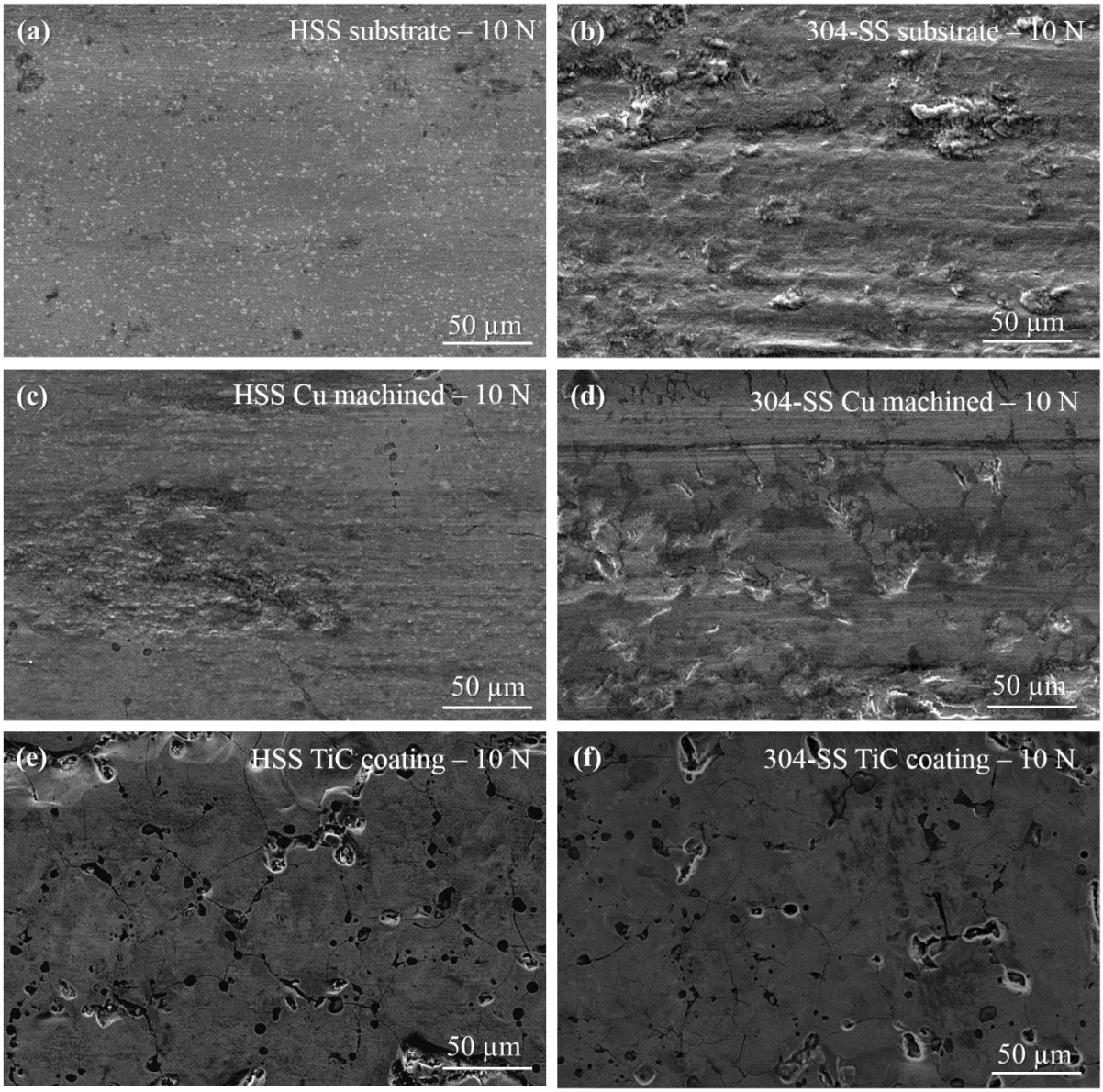

Figure 9 High magnification SE images from the wear tracks of the (a,c,e) HSS and (b,d,f) 304-SS, under conditions of 10 N loading: (a,b) as-polished substrates; (c,d) EDM Cu reference samples; and (e,f) ED cermet coatings.

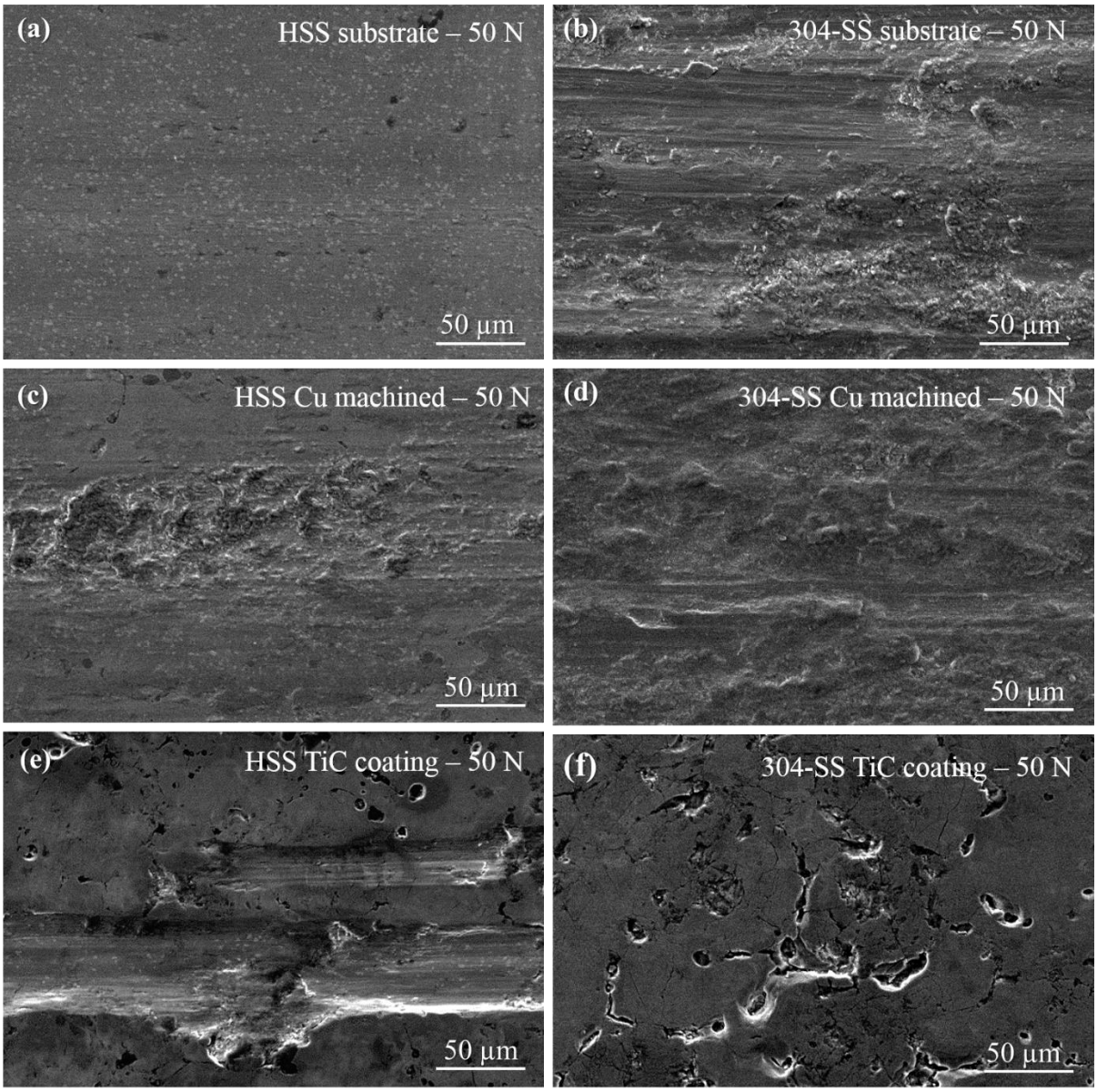

Figure 10 High magnification SE images from the wear tracks of the (a,c,e) HSS and (b,d,f) 304-SS, under conditions of 50 N loading: (a,b) as-polished substrates; (c,d) EDM Cu reference samples; and (e,f) ED cermet coatings.

Figures 10a and 10b illustrate the wear surfaces of the as-polished HSS and 304-SS substrates under the higher loading conditions of 50 N, respectively, demonstrating the same morphologies of the samples under 10 N loading, indicative of the same wear mechanism.

The EDM HSS surface under 50 N loading comprised a mixture of morphologies, including both rough and smooth regions, illustrative of abrasive wear. Conversely, the EDM Cu 304-SS surface exhibited more severe wear, with evidence of significant delamination. EDS analysis of the wear surface again indicated enhanced levels of oxidation, up to ~ 20.7wt%. Both cermet coated HSS and 304-SS substrates under 50 N loading (Figures 11 & 12) showed improved wear performance compared to the as-polished substrates, but exhibited different wear regimes

(cf. Figures 9e&f). Wear tracks on the cermet coated HSS under 50 N load exhibited sharp abrasive grooves developing in the middle of the wear track for almost the entire length of the wear tracks (Figure 11). Figures 11b and 11c show details of sharp abrasive grooves and some embedded debris in this case, characteristic of brittle fracture/grain pull out. Lower levels of oxidation were found to be associated with these worn surfaces (Figures 11b,c; regions I and II; O ~ 4.6 wt% and 4.3 wt %, respectively).

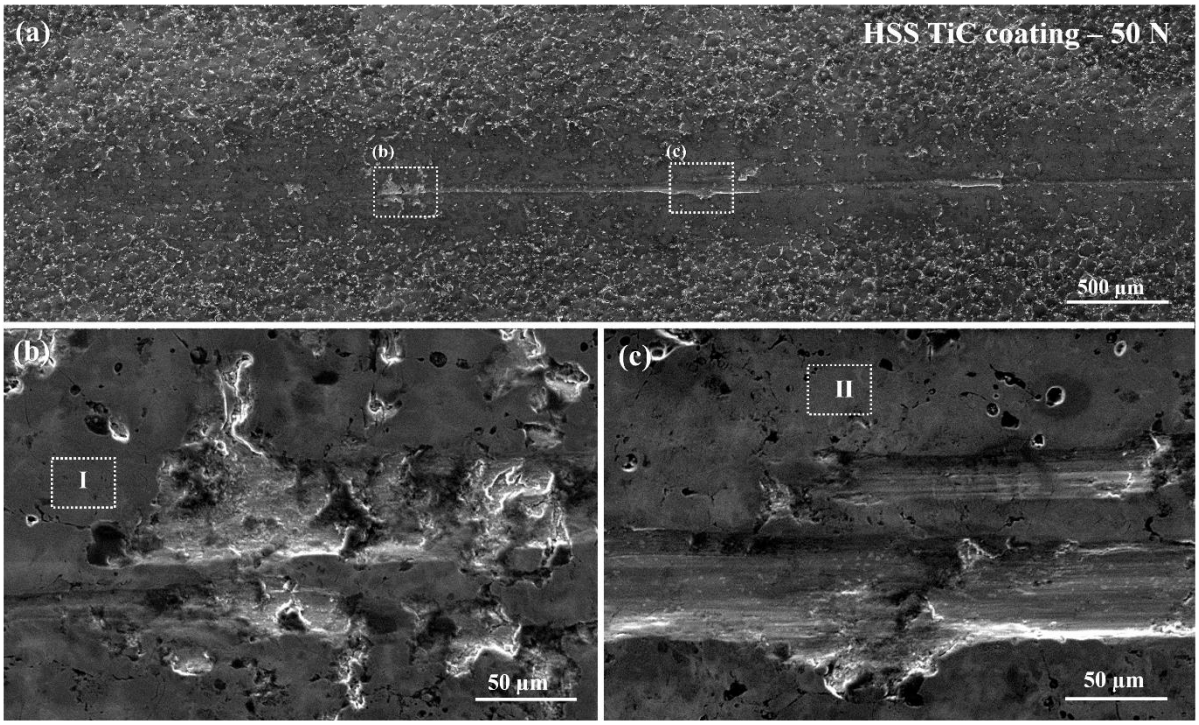

Figure 11 Low magnification SE images showing (a) the extent and (b,c) two representative details of a wear scar on a cermet coated HSS sample, under loading conditions of 50 N, again indicative a greatly improved wear performance.

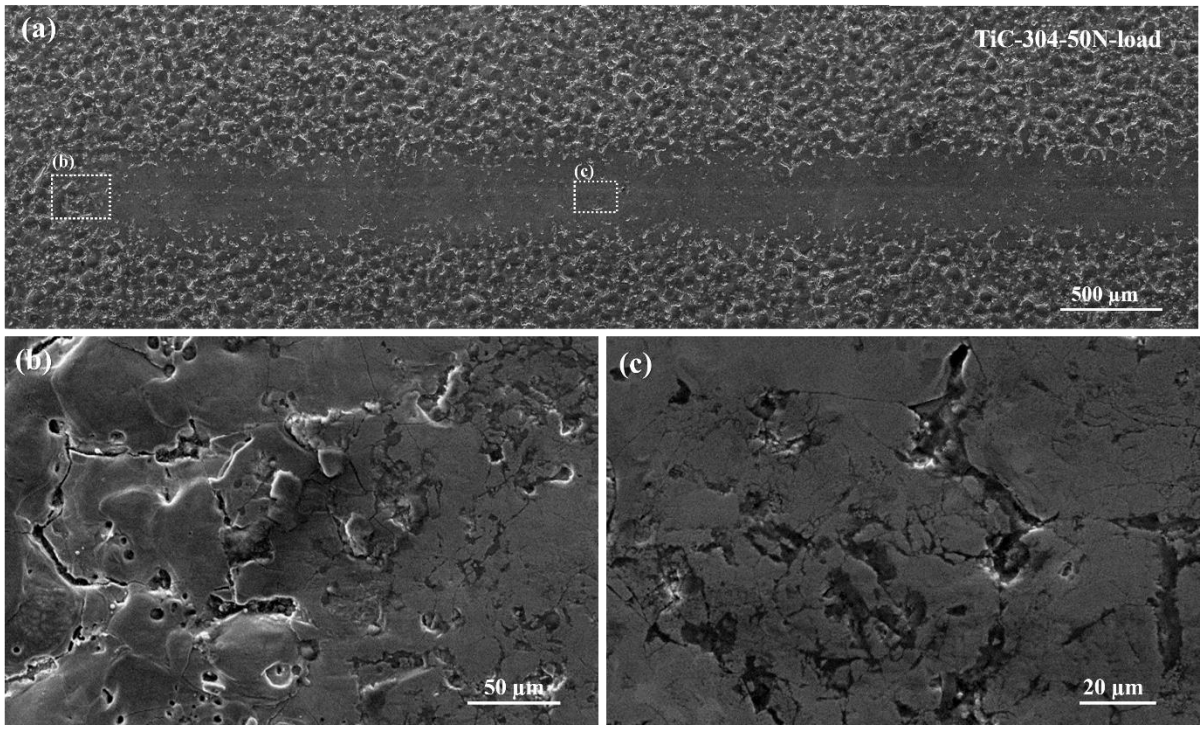

Figure 12 Low magnification SE images showing (a) the extent and (b,c) two representative details of a wear scar on a cermet coated 304-SS sample, under loading conditions of 50 N, again indicative a greatly improved wear performance.

Figure 12 presents a wear scar and highlighted details of cermet coated 304-SS sample under 50 N of loading. The wear track showed evidence of fracture and pull-out of material , the surface exhibited newly developed regions of cracking and micro-cracking (Figures 12b,c), distinct from those remnant from the EDC processing, along with some debris at the ends of the wear tracks.

3.2.3 Counterbody wear rate

The specific wear rates of the counterbodies for all wear tests are shown in figure 13. In the case of all tests using the 304-SS substrate, the counterbody wear rates reflected very closely the trend of the coating wear rate, albeit approximately 1 order of magnitude lower. This lower wear rate is explained by the use of the harder, more wear resistant alpha-alumina counterbody. Additionally the trend of increased sample wear rate with increased load matches the wear rate trend for the counterbodies, except in the case of the TiC coating, in which increasing to 50 N load does not increase counterbody wear significantly. For the HSS based samples, interestingly the counterbody wear rates did not reflect the sample wear rates. In particular, the TiC coating on HSS yielded a slightly higher value of 5.0×10^{-7} mm^3/Nm counterbody wear rate compared to that of the TiC coating on 304-SS of 3.9×10^{-7} mm^3/Nm. This is despite the

notably lower coating wear rate when using a HSS substrate compared to the 304-SS. This phenomenon may be explained by the observed three-body abrasion which is thought to have taken place in samples using the HSS substrate, and has been evidenced by the existence of a sharp abrasive groove in the centre of the wear track on the TiC-HSS coating. Such a phenomenon resulting in localised wear on the coating, but not significantly increase overall wear across the track, is likely to exacerbate counterbody wear.

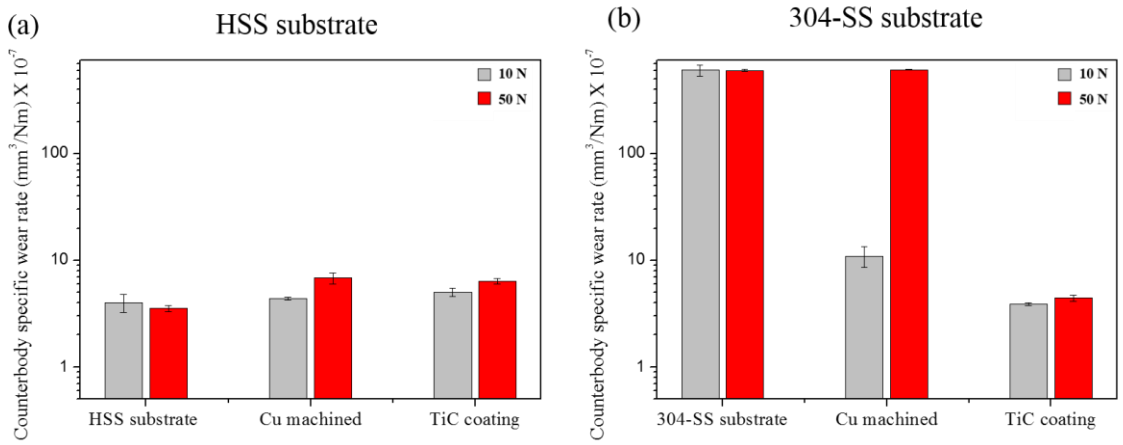

Figure 13 Counterbody Specific wear rates of the Al_2O_3 ball after sliding test against TiC/Fe cermet coating on HSS and 304-SS, both under conditions of 10 and 50 N

3.2.4 Coefficient of friction

Figure 14 presents time dependent coefficient of friction (CoF) profiles, recorded during the wear testing, for the as-polished substrates, the EDM Cu machined surfaces and the TiC/Fe cermet coatings, under conditions of 10 N and 50 N loading. The cermet coated samples, in all cases, yielded lower CoF values, as compared to the as-polished and EDM Cu processed samples. CoF values for cermet coated HSS and 304-SS, once established, under loading conditions of 10 N and 50 N, varied between ~ 0.2 and ~ 0.6. For example, Figure 14a shows the CoF profile for cermet coated HSS under 10 N load, with gradual increase to ~ 0.4 after ~ 160 minutes, at which point steady state friction was achieved. A different onset to the profile was observed for the case of the cermet coated HSS under 50 N load (Figure 14b), with rapid increase of the CoF to ~ 0.7 before dropping to < 0.1, within the first few minutes, as the wear profile initiated. A steep increase in CoF to ~ 0.5 after ~ 15 minutes occurred, as the wear profile became established and thereafter maintained. Conversely, Figure 14c presents the associated CoF profiles for cermet coated 304-SS, under 10 N loading, demonstrating very low CoF values from the outset, up to a steady state value of ~ 0.3. A more gradual increase in the

CoF profile was returned for the cermet coated 304-SS sample under 50 N loading, throughout the duration of the test, reaching a value of ~ 0.55.

The CoF of the as-polished HSS substrate, under conditions of 10 N and 50 N loading (Figures 14a, b), showed initial rapid increase, as the contact area became established, followed by steady state friction of value ~ 0.7 and ~ 0.8, respectively. The CoF of the as-polished 304-SS substrate, under 10 N (Figure 14c), showed similar, initial behaviour, but was noticeably more erratic, returning higher friction values after the initial run-in period. For the case of the 304-SS substrate under 50 N load (Figures 14d), a more steady increase in CoF was observed, reaching a value of ~1.2 by the end of the test.

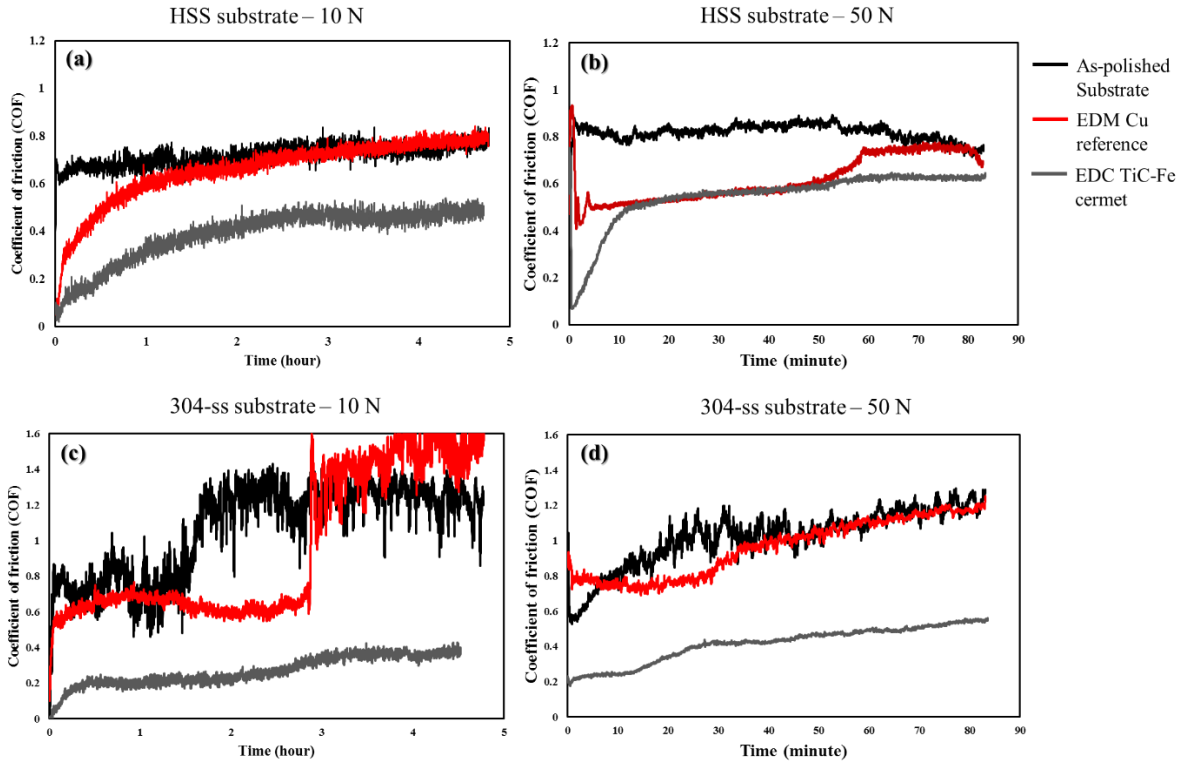

Figure 14 Time dependent coefficient of friction profiles for the as-polished substrates, EDM Cu reference samples, and EDC TiC/Fe cermet samples: a,b) HSS and c,d) 304-SS, both under conditions of 10 and 50 N, respectively

For comparison, the CoF profiles for the EDM Cu processed samples all tended to show intermediate performance between that of the as-polished and cermet coated samples during the early stages of wear, becoming similar to the as-polished samples by the end of the testing. For the case of the Cu processed HSS under 10 N load (Figure 14a), a rapid climb of the CoF to mimic the profile of the as-polished substrate after ~ 90 minutes occurred. When the load

was raised to 50 N, the Cu processed sample, after an initial rapid process of stabilisation, mimicked the performance of the cermet coated HSS sample for about ~ 60 minutes, before a process of degradation to then follow the profile of the as-polished substrate (Figure 14b). The CoF profiles for the Cu processed 304-SS samples showed similar profiles to that of the as-polished substrate, under both loading conditions. However, under 10 N loading conditions (Figure 14c), a noticeable discontinuity in the CoF profiles occurred at ~ 1.5 h and ~ 3 h for the as-polished and Cu processed samples, respectively (Figure 14c).

It is emphasised that the CoF profiles were similar for all repeat tests, with some variations as expected, being applicable to localised surface variations and differing contact behaviour with the wear media.

3.3 Laser processing

Laser surface melting was performed on the TiC/Fe cermet coatings on both substrate types, in order to homogenise the surface. SE imaging of these laser processed surfaces (Figures 15a-d) demonstrated the development of much smoother surfaces, under conditions of both 240 W and 280 W, with significant reduction in the density of pores and cracks, due to reflow of the molten surface, as compared with the as-deposited cermet coatings (Figure 1c,a).

For the case of the HSS substrate, laser treatment at 240 W removed cracks and voids associated with the original ED coating process, but new, relatively large cracks were found to develop (Figure 15a, arrowed). This morphology was distinct from that of the laser processed ED coating on 304-SS (Figure 15c) which yielded a coating entirely free of cracking. The presence and absence of cracks for these laser processed cermet coated HSS and 304-SS was attributed to the different thermal expansion and cooling rate of the coating/substrates system.

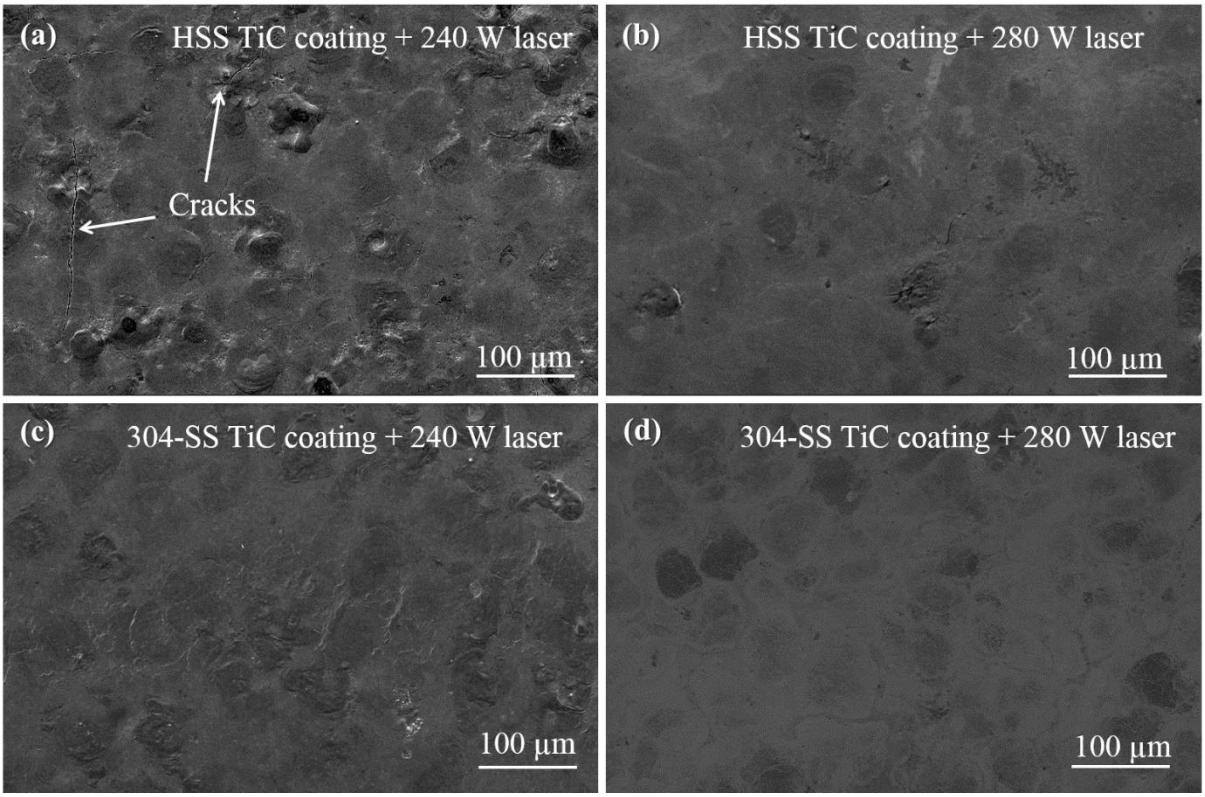

Figure 15 SE images of laser surface treated TiC/Fe cermet coatings on: (a,b) HSS and (c,d) 304-SS substrates, as a function of power: (a,c) 240 W and (b,d) 280 W, respectively (1600 mm/minute scan speed; argon environment).

EDS area analyses indicted that laser processing at 240 W acted to reduce significantly the levels of Ti (TiC) incorporation for both cermet coated HSS and 304-SS samples (from ~ 29 wt% down to ~ 21 wt%; and from ~ 39 wt% down to ~ 26 wt%, respectively). Further, laser processing under conditions of 280 W acted to reduce average Ti (TiC) incorporations down to ~ 15% and ~ 18% respectively.

Table 3 TiC/Fe cermet coating compositions before and after laser treatment, based on EDS area analyses

	Ti Wt%	C Wt%	Fe Wt%	Roughness Ra (µm)		Ti Wt%	C Wt%	Fe Wt%	Roughness Ra (µm)
cermet / HSS	29.3	27.4	30.1	1.2	**cermet / 304-SS**	39.4	31.3	21.1	1.3
cermet / HSS; 240 W laser power	20.8	18.1	41.8	0.4	**cermet / 304-SS; 240 W laser power**	25.6	16.1	40.4	0.3
cermet / HSS; 280 W laser power	15.0	18.7	48.0	0.6	**cermet / 304-SS; 280 W laser power**	18.1	19.8	43.6	0.4

Figure 16 presents low and high-resolution BSE images, in cross-sectional geometry, of TiC/Fe cermets on 304-SS, laser processed under conditions of 240 and 280 W, respectively. Voids and crack formations have been eliminated, for both laser powers, as compared with the original ED cermet coated samples (Figure 2a,c).

The laser processed coatings were characterised by flatter surfaces (Ra ~ 0.26 μm and 0.35 μm for the processes parameter 240 W and 280 W, respectively), and a significant increase in grain size (Figures 16c,d), as compared to the as-deposited cermet coatings (Figure 2a,c), being attributed to an increased melt lifetime, providing for the movement of molten material to in-fill cracks and voids within the coating. The grain structures yielded after laser processing were dendritic in nature, similar to that of laser melted TiC [19].

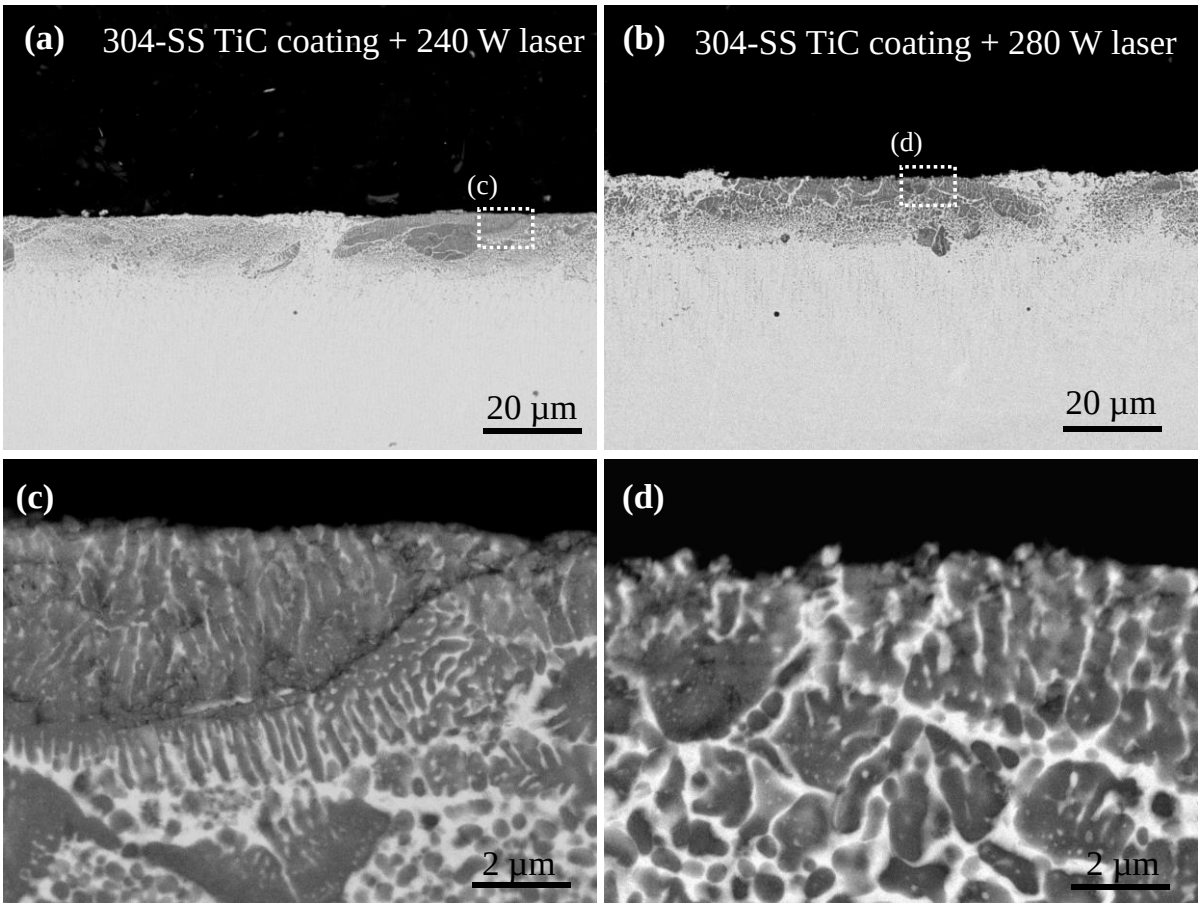

Figure 16 High resolution cross-sectional BSE images of laser surface treated TiC/Fe cermet coatings on 304-SS substrates, as a function of power: (a) 240 W and (b) 280 W, respectively (1600 mm/minute scan speed; argon environment).

3.3.1 Wear behaviour of laser processed EDC cermet coated steels

Figure 17 presents specific wear rate data for cermet coated HSS and 304-SS samples, laser processed at 240 W and 280 W, under identical loading conditions of 10 N and 50 N, for comparison with the as-coated samples (previously described).

Slight improvement in wear rate was returned for the cermet coated HSS under high loading conditions, however the wear rate for HSS under low loading conditions was slightly degraded. Further, the wear rate for all laser processed coatings on 304-SS increased (up to two orders of magnitude) with increasing laser power. For the HSS substrate, a mean wear rate of $0.56x10^{-6}$ mm^3/Nm was returned for the 280 W processed coating using a 50 N load, as compared to 0.64 $x10^{-6}$ mm^3/Nm and 0.87 $x10^{-6}$ mm^3/Nm for the 240 W and untreated coatings, respectively.

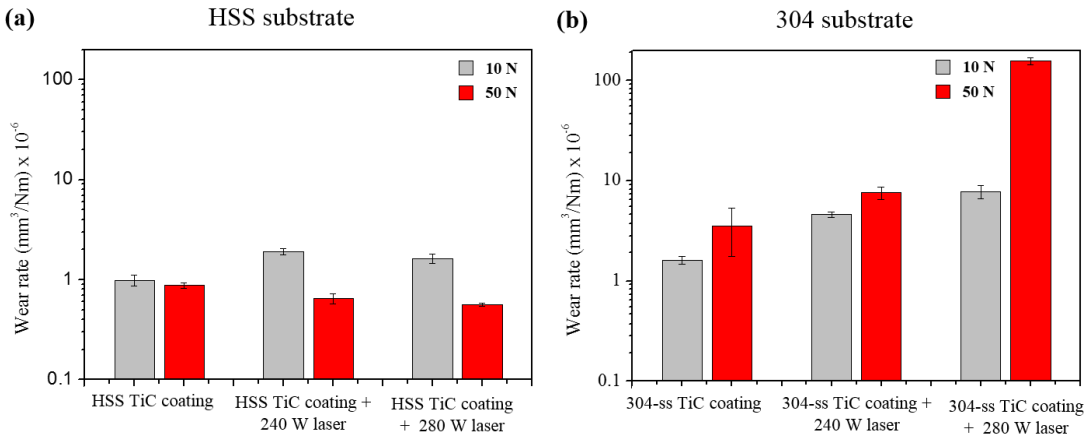

Figure 17 Specific wear rates of as-deposited and laser treated TiC/Fe cermet coatings as a function of power 240 W and, 280 W, under loading conditions of 10 N and 50 N on: a) HSS and b) 304-SS substrates, respectively.

Figure 18 presents SE images of wear track details of 240 W and 280 W laser processed cermet coatings on HSS, showing no significant differences in surface topography. In particular, the sharp grooves and brittle fracture associated with wear scars on as-coated HSS under 50 N loading (Figures 10e and 11a-c) are absent from the laser treated samples, demonstrating the benefit of laser processing for the homogenisation of cermet coated HSS and improved wear performance under high loading conditions. However, for laser processed cermet coated 304-SS, the wear tracks in all cases showed evidence of abrasive grooves characteristic of more severe wear, further the TiC cermet coating processed with 280W laser power is entirely removed at 50 N loading condition, and hence laser processing is considered not beneficial for coatings on more ductile steel substrates.

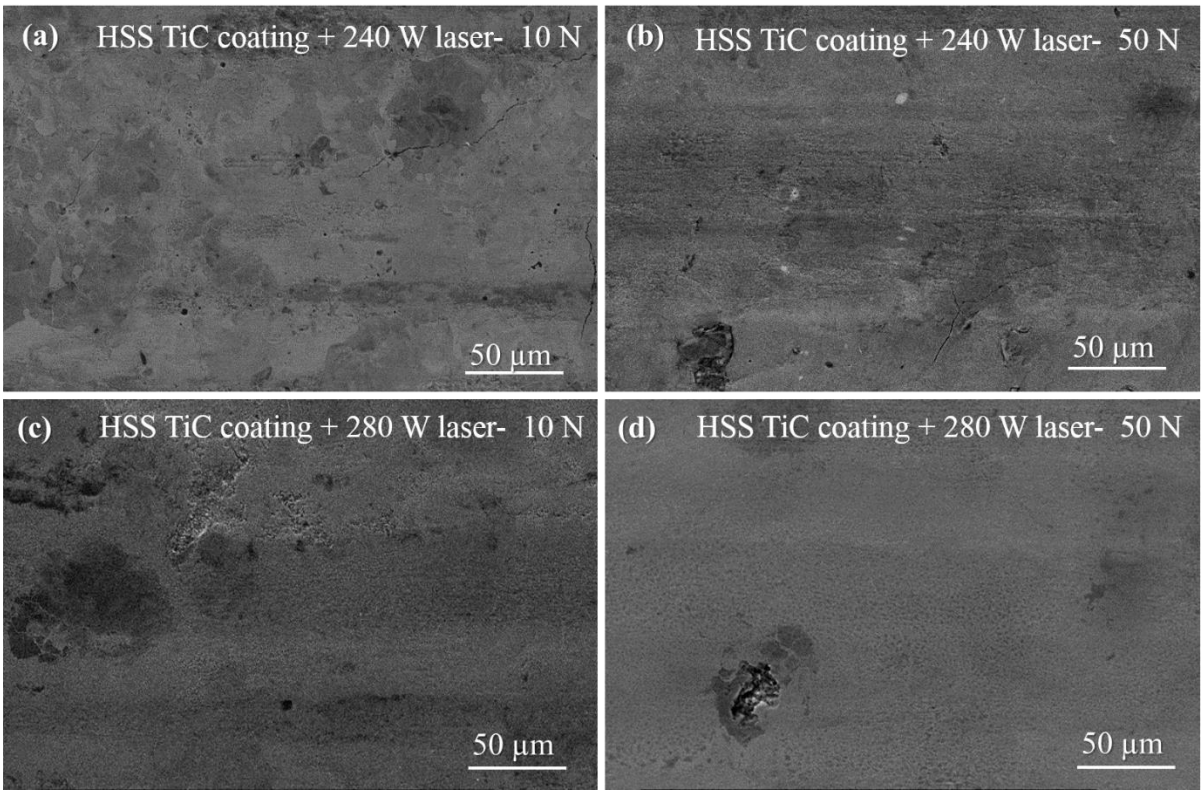

Figure 18 SE micrographs of wear scar details following (a,b) 240 W and (c,d) 280 W laser surface treatment of TiC/Fe cermet coated HSS under loading conditions of (a,c) 10 N; and (b,d) 50 N, respectively (1600 mm/minute scan speed; argon environment).

4 Discussion

This study has shown that the ED TiC/Fe cermet coating of two different steels can yield dry sliding wear resistances up to two orders of magnitude greater than that of the substrate alone (Figure 5), with the variability of specific wear rate reflecting the respective morphologies of the coatings, substrates and loading conditions applied. The lowest wear rate was returned for coated HSS samples under 50 N loading (Figure 5a), whilst best improvement in wear resistance, compared to the as-polished substrate, was shown for coated 304-SS samples under 10 N loading (Figure 5b).

It is interesting to note that the wear rate of cermet coated 304-SS was approximately twice that of coated HSS under loading conditions of 10 N. However, the wear mechanism appeared to be the same for both cermet coated steels under 10 N load, with the production of smooth, wear tracks, mediated by a mechanical polishing mechanism [20]. Further, under conditions of 50 N loading, the wear rate of cermet coated 304-SS was approximately four times that of coated HSS, but with a degradation of wear rate for the 304-SS sample, as compared with a slight improvement in wear rate for the HSS sample, respectively, reflecting a difference in the

wear mechanism under conditions of higher loading. This point is particularly notable, given the level of TiC present in the coating on 304-SS (Ti 39wt%) was significantly higher than for coated HSS (29 wt%) (Table 3)). Hence, it is evident that the substrate has a strong influence on the wear performance of cermet coated steels.

The dependence of wear behaviour on coating/substrate properties may be explained with reference to the microstructures and properties of the TiC/Fe coatings and the steel substrates. The fine details of the microstructures of the coatings on both steel substrates investigated in this study are revealed in cross-sectional geometry in Figures 2 and 3. It is recognised that these TiC-based coatings comprise a complex intermix of a Fe-based matrix with TiC grains, of varying sizes and geometries, depending on depth into the coating [4, 5]. Hence, it is logical that the final mechanical properties of the coating comprise those of the individual TiC and Fe phases. Particularly given the much poorer wear behaviour of pure 304-SS compared to HSS, the poorer wear behaviour of the TiC coating on 304-SS can generally be explained by the much lower hardness of 304-SS (196 HV; σ = 16.8) in comparison to that of HSS (733 HV; σ = 94), hence providing poorer wear properties to the final coating. The authors have previously measured hardness of ~1800 HV for TiC coatings, using identical conditions to this work, on 304 stainless steel [4]. When we consider this hardness level, the contribution of a matrix from a much softer steel (196 HV compared to 733 HV for HSS), is thought to provide a significant impact on mean coating mechanical properties, and hence wear behaviour. The pervasive nature of the substrate as a matrix inside the coating, evidenced by the highly composite nature of the coatings (as shown in Figure 2 and 3), also supports the substrate properties contributing significantly to final coating properties.

The contribution of a second mechanism to the wear behaviour cannot be ruled out, in which deflection of the coating, caused by deformation of the underlying, substrate, results in deflection of the coating, in turn leading to an increase in wear rate [21]. Hence, also in this case, a softer substrate would contribute to an increased wear rate.

The TiC/Fe coating on HSS, under 50 N loading, exhibited signs of fracture and grain pull-out (Figure 11), with the wear tracks comprising long, sharp, abrasive grooves, indicative of either debris trapped between counterbody and substrate, or debris adhered to the counterbody. This phenomenon, typical of an abrasive wear mechanism, is well understood with entrapped, hard/sharp, relatively large, ceramic particles acting as abrasive particles or moving indents,

causing scratching [14, 22, 23]. This wear mechanism differs from that of the cermet coated 304-SS, under 50 N loading, whereby pull-out of material and crack formation without debris-based characteristic abrasive grooving were dominant.

It is noted that the specific wear rates of these ED TiC/Fe cermet coated steels, produced using a semi-sintered TiC tool electrode (~1- 0.9 $x10^{-6}$ on HSS and ~ 1.6 - 3.6 $x10^{-6}$ mm^3/Nm on 304-SS, under 10 N and 50 N loads, respectively), are significantly lower than those reported for TiC-based coatings produced using a semi-sintered Ti tool electrode, with and without graphite mixed dielectric fluid (5.8 - 8 $x10^{-6}$ mm^3/Nm and 24.6 - 150 x 10^{-6} mm^3/Nm, under 20 N and 50 N loads, respectively), on 45# carbon steel, based on wear tests of 15 minutes duration using a 6 mm Si_3N_4 ball at room temperature [7]. This demonstrates that the direct ED production of TiC/Fe using a TiC tool electrode provides for coatings with enhanced wear resistance compared to cermet coatings produced via the *in-situ* reaction of Ti with C.

Compared to other coating methods, the range of specific wear rates observed using EDC here from a semi-sintered TiC electrode is broadly consistent with various TiC thin coating systems. For example, a magnetron sputtered nanocrystalline TiC/amorphous C composite thin film coating yielded a wear rate of ~2 – 4 x 10^{-6} mm^3/Nm at room temperature for coatings in the range of 0.5 < C/Ti < 1.5 wt% ratio at 1 and 5 N loading condition [22]. In addition, a comparison can be made with the same cermet material system under identical reciprocating ball-on-flat geometry, to the present work. For example, Onuoha et al. [24] report a variable specific wear rate for TiC–304L stainless steel composites prepared by melt infiltration of ~ 4 – 24 x 10^{-7} mm^3/Nm, when worn against 6.35 mm diameter WC–Co balls for a load range of 20 to 80 N load.

It is also interesting to note that EDC processing imparted superior wear resistance to the steels, as compared with EDM processed surfaces using a reference Cu tool electrode. EDM surfaces subjected to wear testing under identical conditions yielded similar wear rates to those of the as-polished substrates (Figure 5), with the exception of the processed 304-SS under 10 N loading which showed an order of magnitude improvement in specific wear rate. This latter observation was attributed to some hardening of the sample near surface upon crystallization following EDM processing, thereby increasing the effective wear resistance of the sample compared to the as-polished 304-SS. No additional benefit was imparted by EDM into the HSS given its initial, higher wear resistance.

An additional processing step of laser surface treatment was used in order to improve the surface morphology of the ED TiC/Fe coatings, whilst seeking to maintain wear performance. Under laser power conditions of 280 W, cracking and porosity were almost eliminated from the coating surfaces for both substrate types.

However, with regard to the wear performance of laser processed ED coatings on HSS, a minimal reduction in wear rate was returned only for the higher loading condition of 50 N, with a slight increase in wear rate under 10 N (Figure 17a). The reason for improvement in wear performance under higher loading may be attributed to surface homogenisation (Figures 15a,b) and the removal of asperities which would otherwise induce stress concentrations and localised fracture (Figure 11). Conversely, diminished wear performance under the lower loading conditions of 10 N may be attributed to a reduction in the Tiwt% content of the coating, as a consequence of laser processing (Table 3), which would act to reduce hardness [4].

Intriguingly, for the case of laser processed TiC/Fe coatings on 304-SS, the wear rate degraded significantly in all cases (Figure 17b). This phenomenon may be explained with reference to the initial wear properties of the softer 304-SS, coupled with a reduction of the Tiwt% content of the coating, from ~39wt% (as-deposited), to ~25wt% (240 W laser power) and ~18wt% (280 W laser power), respectively (Table 3). Further, the BSE images of Figure 16 indicated an increase in coating grain size (compared to Figure 2), as a consequence of laser treatment, indicative of a slower cooling rate during the process of recrystallisation, which might also contribute to a modification of coating mechanical properties and hence wear performance. Accordingly, laser processing of EDC cermet layers acts to lower the ceramic content, being diluted with base metal, such that wear performance then becomes dominated by the properties of the substrate.

5 Conclusions

TiC/Fe cermets have been produced on HSS and 304-SS substrates using the electrical discharge coating (EDC) process with a semi-sintered TiC tool electrode. The as-deposited coatings exhibited complex, TiC/Fe cermet microstructures, with a mixture of equiaxed and banded columnar grains near the surface, and coarse to finely graded equiaxed grains towards the coating / substrate interface, reflecting the final cool-down sequence of ED processing. The

cermet coatings on HSS and 304-SS yielded wear rates, under dry sliding conditions, one and two orders of magnitude lower than those of the as-polished substrates. In particaulr, wear performance was found to be dependent strongly on substrate type, with coatings on HSS being ~ 2-4 times more wear resistant than those on 304-SS. The variability of wear rate was attributed to a combination of factors, being dependent on the morphology of the cermet coatings combined with the mechanical properties of the substrate. An additional processing step of laser surface treatment was used to homogenise the ED cermet coatings, with conditions of 280 W laser power eliminating successfully all cracking and porosity characteristic of the as-deposited coatings. However, laser processing was associated with a general increase in wear rate for all samples, with the exception of HSS under high loading conditions. This effect was attributed to a dilution of the amount of TiC within the cermet coatings, following laser processing combined with an increase in grain size. Improvement of the wear rate of laser-treated, cermet coated HSS, under conditions of high loading, as attributed to the avoidance of abrasive wear mechanisms following homogenisation of the coating.

Acknowledgments

Samer J. Algodi thanks the Ministry of Higher Education & Scientific Research in Iraq for funding support. A.T. Clare would like to acknowledge funding from Engineering and Physical Sciences Research Council [grant number EP/L017547/1]. In addition, the authors acknowledge the kind support of Mr Iwasaki of Mitsubishi Electric Nagoya.

References

1. Wang, Z.L., et al., *Surface modification process by electrical discharge machining with a Ti powder green compact electrode.* Journal of Materials Processing Technology, 2002. **129**(1–3): p. 139-142.
2. Zhu, H., et al., *Reaction mechanisms of the TiC/Fe composite fabricated by exothermic dispersion from Fe–Ti–C element system.* Powder technology, 2013. **246**: p. 456-461.
3. Rajabi, A., et al., *Development and application of tool wear: A review of the characterization of TiC-based cermets with different binders.* Chemical Engineering Journal, 2014. **255**: p. 445-452.
4. Algodi, S.J., et al., *Electrical discharge coating of nanostructured TiC-Fe cermets on 304 stainless steel.* Surface and Coatings Technology, 2016. **307**: p. 639-649.
5. Murray, J.W., et al., *Formation mechanism of electrical discharge TiC-Fe composite coatings.* Journal of Materials Processing Technology, 2017. **243**: p. 143-151.
6. Hwang, Y.-L., C.-L. Kuo, and S.-F. Hwang, *The coating of TiC layer on the surface of nickel by electric discharge coating (EDC) with a multi-layer electrode.* Journal of Materials Processing Technology, 2010. **210**(4): p. 642-652.

7. Xie, Z., et al., *Titanium carbide coating with enhanced tribological properties obtained by EDC using partially sintered titanium electrodes and graphite powder mixed dielectric.* Surface and Coatings Technology, 2016. **300**: p. 50-57.
8. ZENG, Z.-y., et al., *Friction and wear behaviors of TiCN coating based on electrical discharge coating.* Transactions of Nonferrous Metals Society of China, 2015. **25**(11): p. 3716-3722.
9. Sova, A., et al., *Cold spray deposition of 316L stainless steel coatings on aluminium surface with following laser post-treatment.* Surface and Coatings Technology, 2013. **235**: p. 283-289.
10. Afzal, M., et al., *Effect of laser melting on plasma sprayed WC-12wt.% Co coatings.* Surface and Coatings Technology, 2015. **266**: p. 22-30.
11. Algodi, S.J., A.T. Clare, and P.D. Brown, *Modelling of single spark interactions during electrical discharge coating.* Journal of Materials Processing Technology, 2018. **252**: p. 760-772.
12. Kain, V., et al., *Effect of cold work on low-temperature sensitization behaviour of austenitic stainless steels.* Journal of Nuclear Materials, 2004. **334**(2): p. 115-132.
13. Varez, A., et al., *Sintering in different atmospheres of T15 and M2 high speed steels produced by a modified metal injection moulding process.* Materials Science and Engineering: A, 2004. **366**(2): p. 318-324.
14. Azadi, M., et al., *Mechanical behavior of TiN/TiC multilayer coatings fabricated by plasma assisted chemical vapor deposition on AISI H13 hot work tool steel.* Surface and Coatings Technology, 2014. **245**: p. 156-166.
15. Yoon, K., et al., *Wear mechanism of TiN-coated high-speed steel during sliding.* Wear, 1993. **170**(1): p. 101-108.
16. Telasang, G., et al., *Wear and corrosion behavior of laser surface engineered AISI H13 hot working tool steel.* Surface and Coatings Technology, 2015. **261**: p. 69-78.
17. Sun, Y., *Sliding wear behaviour of surface mechanical attrition treated AISI 304 stainless steel.* Tribology International, 2013. **57**: p. 67-75.
18. Hsu, C.-H., K.-H. Huang, and Y.-H. Lin, *Microstructure and wear performance of arc-deposited Ti–N–O coatings on AISI 304 stainless steel.* Wear, 2013. **306**(1): p. 97-102.
19. Gu, D., et al., *Nanocrystalline TiC reinforced Ti matrix bulk-form nanocomposites by Selective Laser Melting (SLM): Densification, growth mechanism and wear behavior.* Composites Science and Technology, 2011. **71**(13): p. 1612-1620.
20. Jin, C., et al., *Microstructural damage following reciprocating wear of TiC-stainless steel cermets.* Tribology International, 2017. **105**: p. 201-218.
21. Holmberg, K. and A. Matthews, *Coatings Tribology: Properties, Mechanisms, Techniques and Applications in Surface Engineering*. 2009: Elsevier Science.
22. Souček, P., et al., *Tribological properties of nc-TiC/aC: H coatings prepared by magnetron sputtering at low and high ion bombardment of the growing film.* Surface and Coatings Technology, 2014. **241**: p. 64-73.
23. Arun, I., et al., *Synthesis of electric discharge alloyed nickel–tungsten coating on tool steel and its tribological studies.* Materials & Design, 2014. **63**: p. 257-262.
24. Onuoha, C.C., et al., *The reciprocating wear behaviour of TiC–304L stainless steel composites prepared by melt infiltration.* Wear, 2013. **303**(1): p. 321-333.

Figure captions

Figure 1 SE images of (a,c) ED cermet coatings; and (b,d) EDM Cu reference samples on 304-SS and HSS substrates, respectively.

Figure 2 Cross-sectional BSE images of a TiC/Fe cermet ED coating on 304-SS (TiC deposited under conditions of 10 A current and 8 µs pulse-on time), showing the development of a banded, composite microstructure.

Figure 3 Cross-sectional BSE images of a TiC/Fe cermet ED coating on HSS (TiC deposited under conditions of 10 A current and 8 µs pulse-on time), showing the development of a similar, variable, composite microstructure.

Figure 4 XRD patterns for ED processed TiC/Fe cermet coatings on (a) 304-SS and (b) HSS substrates, along with reference Cu machined surfaces.

Figure 5 Specific wear rates (logarithmic scale) for samples based on: a) HSS and b) 304-SS substrates (as-polished substrate; EDM Cu reference surface; and EDC TiC/Fe cermet coating) under loads of 10 N and 50 N, respectively.

Figure 6 Cross-sectional wear scars profiles for the as-polished substrates, EDM Cu reference samples, and EDC TiC/Fe cermet samples: a,b) HSS and c,d) 304-SS, both under conditions of 10 and 50 N, respectively.

Figure 7 Low magnification SEM images showing (a) the extent (mixed SE & BSE image) and (b,c) representative details of a wear scar on an as-polished HSS substrate under loading conditions of 10 N, indicative of abrasive wear (SE image).

Figure 8 Low magnification SE images showing (a) the extent and (b,c) two representative details of a wear scar on a cermet coated HSS sample, under loading conditions of 10 N, indicative a greatly improved wear performance.

Figure 9 High magnification SE images from the wear tracks of the (a,c,e) HSS and (b,d,f) 304-SS, under conditions of 10 N loading: (a,b) as-polished substrates; (c,d) EDM Cu reference samples; and (e,f) ED cermet coatings.

Figure 10 High magnification SE images from the wear tracks of the (a,c,e) HSS and (b,d,f) 304-SS, under conditions of 50 N loading: (a,b) as-polished substrates; (c,d) EDM Cu reference samples; and (e,f) ED cermet coatings.

Figure 11 Low magnification SE images showing (a) the extent and (b,c) two representative details of a wear scar on a cermet coated HSS sample, under loading conditions of 50 N, again indicative a greatly improved wear performance.

Figure 12 Low magnification SE images showing (a) the extent and (b,c) two representative details of a wear scar on a cermet coated 304-SS sample, under loading conditions of 50 N, again indicative a greatly improved wear performance.

Figure 13 Counterbody Specific wear rates of the Al_2O_3 ball after sliding test against TiC/Fe cermet coating on HSS and 304-SS, both under conditions of 10 and 50 N

Figure 14 Time dependent coefficient of friction profiles for the as-polished substrates, EDM Cu reference samples, and EDC TiC/Fe cermet samples: a,b) HSS and c,d) 304-SS, both under conditions of 10 and 50 N, respectively

Figure 15 SE images of laser surface treated TiC/Fe cermet coatings on: (a,b) HSS and (c,d) 304-SS substrates, as a function of power: (a,c) 240 W and (b,d) 280 W, respectively (1600 mm/minute scan speed; argon environment).

Figure 16 High resolution cross-sectional BSE images of laser surface treated TiC/Fe cermet coatings on 304-SS substrates, as a function of power: (a) 240 W and (b) 280 W, respectively (1600 mm/minute scan speed; argon environment).

Figure 17 Specific wear rates of as-deposited and laser treated TiC/Fe cermet coatings as a function of power 240 W and, 280 W, under loading conditions of 10 N and 50 N on: a) HSS and b) 304-SS substrates, respectively.

Figure 18 SE micrographs of wear scar details following (a,b) 240 W and (c,d) 280 W laser surface treatment of TiC/Fe cermet coated HSS under loading conditions of (a,c) 10 N; and (b,d) 50 N, respectively (1600 mm/minute scan speed; argon environment).

Table captions

Table 1 EDC processing parameters
Table 2 Chemical composition of the starting 304-SS and HSS substrates
Table 3 TiC/Fe cermet coating compositions before and after laser treatment, based on EDS area analyses